NeuroImage 305 (2025) 120951

Contents lists available at ScienceDirect

NeuroImage

journal homepage: www.elsevier.com/locate/ynimg

Exploring the impact of APOE ε4 on functional connectivity in Alzheimer's disease across cognitive impairment levels

Kangli Dong [a,1], Wei Liang [a,1], Ting Hou [b,1], Zhijie Lu [c], Yixuan Hao [c], Chenrui Li [c], Yue Qiu [c], Nan Kong [c], Yan Cheng [d], Yaqi Wen [e], Wanyin Ma [e], Wenbin Zheng [e], Jitian Guan [e], Yan Lin [e], Kai Huang [e], Lu Zhang [f], Siya Chen [g], Xiangyuan Ma [a,*], Renhua Wu [e,*], Naili Wei [c,*], for the Alzheimer's Disease Neuroimaging Initiative [2]

[a] Department of Biomedical Engineering, College of Engineering, Shantou University, Shantou, 515063, Guangdong, China
[b] Department of Human Anatomy and Physiology, Zhongshan School of Medicine, Sun Yat-Sen University, Guangzhou, 510080, Guangdong, China
[c] Department of Neurosurgery, The First Affiliated Hospital of Shantou University Medical College, Shantou, 515041, Guangdong, China
[d] The Second Hospital of Shandong University, Jinan, 250033, Shandong, China
[e] Department of Radiology, The Second Affiliated Hospital of Shantou University Medical College, Shantou, 515000, Guangdong, China
[f] Department of Rehabilitation, Sir Run Run Shaw Hospital, Zhejiang University School of Medicine, Zhejiang University, Hangzhou, 310027, Zhejiang, China
[g] Department of Computer Science, City University of Hong Kong, Hong Kong, 999077, Hong Kong, China

ARTICLE INFO

Dataset link: adni.loni.usc.edu

Keywords:
Alzheimer
APOE ε4
fMRI
Functional connectivity
Graph neural network

ABSTRACT

The apolipoprotein E (APOE) ε4 allele is a recognized genetic risk factor for Alzheimer's Disease (AD). Studies have shown that APOE ε4 mediates the modulation of intrinsic functional brain networks in cognitively normal individuals and significantly disrupts the whole-brain topological structure in AD patients. However, how APOE ε4 regulates brain functional connectivity (FC) and consequently affects the levels of cognitive impairment in AD patients remains unknown. In this study, we systematically analyzed functional magnetic resonance imaging (fMRI) data from two distinct cohorts: an In-house dataset includes 59 AD patients (73.37 $\pm$ 6.42 years), and the ADNI dataset includes 117 AD patients (74.91 $\pm$ 7.91 years). Experimental comparisons were conducted by grouping AD patients based on both APOE ε4 status and cognitive impairment levels of AD. Network-Based Statistic (NBS) method and the Graph Neural Network Explainer (GNN-Explainer) were combined to identify significant FC changes across different comparisons. Importantly, the GNN-Explainer method was introduced as an enhancement over the NBS method to better model complex high-order nonlinear characteristics for discovering FC features that significantly contribute to classification tasks. The results showed that APOE ε4 primarily influenced temporal lobe FCs, while it influenced different cognitive impairment levels of AD by adjusting prefrontal-parietal FCs. These findings were validated by p-values < 0.05 from NBS method, and 5-fold cross-validation along with ablation studies from the GNN-Explainer method. In conclusion, our findings provide new insights into the role of APOE ε4 in altering FC dynamics during the progression of AD, highlighting potential targets for early intervention.

1. Introduction

APOE ε4 is a variant allele of the APOE gene, and is considered one of the most significant genetic risk factors for Alzheimer's disease (AD) (Genin et al., 2011). Carriers of the APOE ε4 allele are associated with a greater risk of developing AD (Liu et al., 2013; Bertram et al., 2010), and have a younger average age of onset compared to non-carriers (Corder et al., 1993). Evidence from both cognitive-behavioral and neuroimaging studies has demonstrated that APOE ε4 has significant impacts on various cognitive functions in individuals with AD. Studies have shown that carriers of the APOE ε4 allele exhibit more impaired memory functions (Van der Flier et al., 2006) and greater

* Corresponding authors.
E-mail addresses: maxiangyuan@stu.edu.cn (X. Ma), rhwu@stu.edu.cn (R. Wu), nlwei@stu.edu.cn (N. Wei).

[1] Equal contribution.

[2] Data used in preparation of this article were obtained from the Alzheimer's Disease Neuroimaging Initiative (ADNI) database (adni.loni.usc.edu). As such, the investigators within the ADNI contributed to the design and implementation of ADNI and/or provided data but did not participate in analysis or writing of this report. A complete listing of ADNI investigators can be found at: http://adni.loni.usc.edu/wp-content/uploads/how_to_apply/ADNI_Acknowledgement_List.pdf.

https://doi.org/10.1016/j.neuroimage.2024.120951
Received 22 September 2024; Received in revised form 16 November 2024; Accepted 19 November 2024
Available online 4 December 2024

medial temporal lobe atrophy (Agosta et al., 2009). In contrast, non-carriers of the APOE ε4 allele experience more severe impairment in executive functions and exhibit greater frontal lobe atrophy (Wolk et al., 2010).

When disregarding the APOE ε4 factor, the mechanism of AD on the brain is commonly considered to be a disconnection syndrome that can disrupt brain network structures (Delbeuck et al., 2003). Brain networks refer to the patterns of connections and interactions between different regions of the brain at functional, structural, or computational levels, which follow the principles of network science, viewing the brain as a complex network composed of multiple nodes (brain regions) and edges (neural fibers or functional connectivities (FC)) (Bassett and Sporns, 2017). The human brain has been found to exhibit small-world properties or a topological network structure composed of highly connected hubs (Bullmore and Sporns, 2009). Research of the impact of AD on brain networks suggests that even if AD pathology initially presents in localized brain regions, it can still affect the topological structure of the entire brain network (Dai et al., 2019; John et al., 2017). Specifically, AD is found to lead to a loss of balance between the separation and integration of brain information, as well as a reorganization of network hubs that regulate the flow of information (Lo et al., 2010; Stam et al., 2007; Sanabria-Diaz et al., 2013), culminating in disrupting the network topology of brain networks (Wang et al., 2013).

Several studies have also explored the changes in brain network structure when considering the APOE ε4 allele. Part of these studies focus on exploring the changes in FC patterns induced by the APOE ε4 factor: For instance, Fleisher et al. (2009) found that FC in several brain regions (prefrontal, orbitofrontal, temporal, and parietal lobes, et al.) can differentiate between normal APOE ε4 carriers and non-carriers. Filippini et al. (2009) reported that APOE ε4 carriers exhibit increased co-activation in the default mode network (DMN), involving the posterior cingulate, medial temporal, and medial prefrontal cortex regions, compared to non-carriers. Goveas et al. (2013) found that while FC in the DMN and executive control network (ECN) is predominantly reduced, there is a significant enhancement in the FC between the salience network (SN) and DMN for APOE ε4 carriers. Koelewijn et al. (2019) discovered a low-connectivity brain network in AD patients, which partially overlaps with hyperconnected regions observed in younger APOE ε4 carriers. Brown et al. (2011) found that compared to non-carriers of APOE ε4, carriers of APOE ε4 exhibit an accelerated age-related decline in the average local interconnectivity of brain networks, with decreases in regional local interconnectivity in the precuneus, medial orbitofrontal cortex, and lateral parietal cortex. Other studies emphasize the investigation of alterations in brain network topology resulting from APOE ε4 factor: Ma et al. (2017) identified significant interactions between the APOE ε4 factor and mild cognitive impairment (MCI) in the clustering coefficients and local efficiency of brain networks related to general cognitive function and white matter connectivity. Clarke et al. (2022) found no effects of APOE ε4 factor on graph-theoretical metrics in the structural brain networks of cognitively healthy individuals; however, APOE ε4 was associated with hubs in the right paracentral lobule, which is linked to motor and sensory functions in the medial frontal-parietal cortical regions. Mirza-Davies et al. (2022) found that APOE ε4 is associated with a reduction in the average node strength of the rich club in both visual subnetworks and the whole-brain structural network. Goryawala et al. (2015) found that compared to non-carriers of APOE ε4, carriers of APOE ε4 exhibit an abnormal small-world structure in the cortical network of the brain, with increased clustering coefficients and path lengths, indicating poorer topological architecture of brain networks. For patients with AD, APOE ε4 has been found to reduce the efficiency of parallel information transfer, diminish the modular connectivity within the posterior DMN (pDMN) as well as between pDMN and the ECN, and disrupt the functional hubs and rich-club organizations that primarily involve brain regions such as the pDMN, ECN, and the sensorimotor systems (Wang et al., 2015a).

Table 1
Comparison of key characteristics: In-house Dataset vs ADNI Dataset.

Characteristics	In-house Dataset	ADNI Dataset
Number of subjects	59 subjects	117 subjects
Age (mean ± SD)	73.37 ± 6.42 years	74.91 ± 7.91 years
Gender distribution	18 males, 41 females	59 males, 58 females
Imaging modalities	T1-weighted MRI, fMRI	T1-weighted MRI, fMRI
fMRI modalities	Resting-State fMRI	Resting-State fMRI, Extended Resting-State fMRI, Axial Resting-State fMRI (Eyes Open)
MRI scanner and sequence	3.0T MRI scanner (Signa, GE Healthcare) for Spin echo (SE) sequence for T1-weighted imaging	Various MRI sequence (e.g., MPRAGE SENSE2, MPRAGE GRAPPA2, etc.)

Research on AD staging contributes to the standardization of AD diagnosis and reveals the natural history of AD (Therriault et al., 2024). Although existing research has started to explore the impact of the APOE ε4 factor on the topological structure of brain networks, its effects on different cognitive impairment levels in AD (mild, moderate, and severe staging) are currently not well understood. Addressing this problem is crucial for helping our understanding of how APOE ε4 progressively impacts network topology and functional integrity, thereby providing a theoretical basis and guidance for developing interventions to prevent the worsening of the condition. In this investigation, both APOE ε4 and the cognitive impairment levels of AD were considered simultaneously. By comparing different groups (APOE ε4 carriers and non-carriers; mild, moderate, and severe AD; mild, moderate, and severe AD within carriers), we aimed to explore the different FC patterns of how APOE ε4 and cognitive impairment levels of AD influence brain network communication. Furthermore, we introduced an interpretable deep learning model beyond statistical analysis to discover FC features that contribute significantly to classification tasks.

The remainder of the paper is organized as follows: Section 2 provides an overview of the dataset and introduces the proposed framework. Section 3 reports the experiments, results, and key findings. Finally, the paper concludes with a discussion and a brief conclusion in Sections 4 and 5.

2. Methods

This section presents the framework for identifying significant brain FCs for different comparison scenarios considering both APOE ε4 and cognitive impairment levels, as illustrated in Fig. 1. The framework processes fMRI images to generate significant FC outcomes using both the Network-Based Statistic (NBS) method and the Graph Neural Network Explainer (GNN-Explainer) method. It begins by detailing the preprocessing steps for fMRI images, which are used to construct FC matrices and analyze node features. The processing of FCs is then performed in parallel for different comparison groups using the NBS method and the GNN-Explainer method.

2.1. fMRI datasets

In-house dataset

The in-house dataset was collected at the collaborating hospital following the approval of the institutional review board (IRB), with ethics approval granted under the code 2020-115-XZ2 by the First Affiliated Hospital of Shantou University Medical College. Each patient underwent both fMRI and MRI scans upon admission, and APOE genotype information was collected, along with Mini-Mental State Examination (MMSE) scores to assess cognitive impairment levels. Additionally, demographic data were collected, including age (mean:

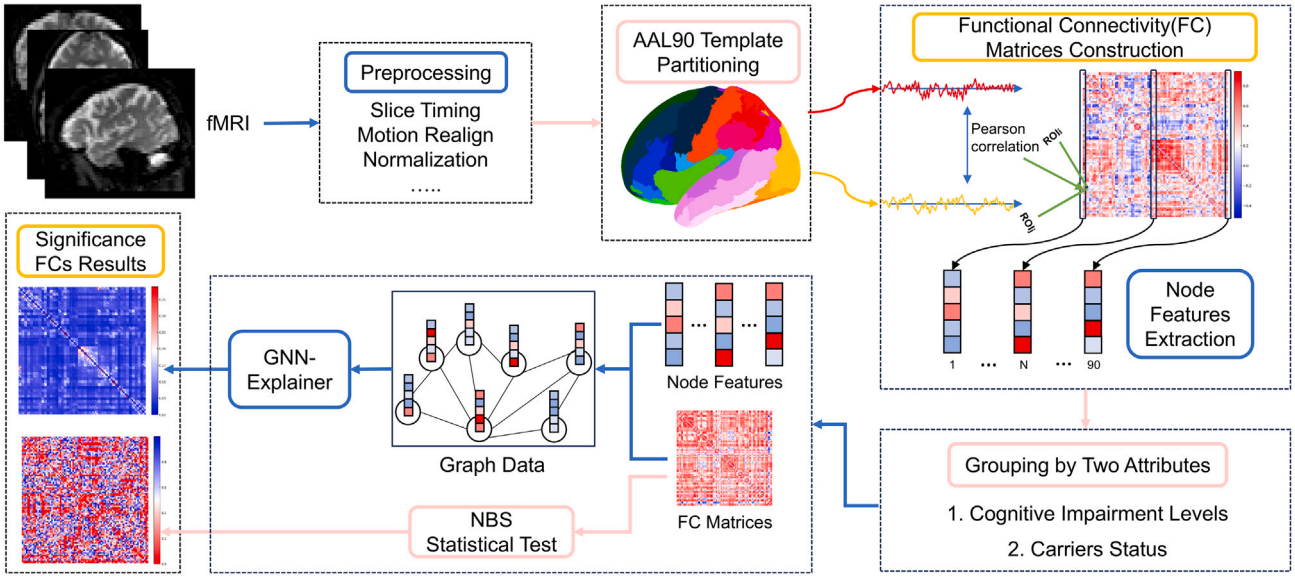

Fig. 1. Overview of the framework for identifying significant connections. The framework consists of several key steps: preprocessing to generate FC matrices and node features, categorizing participants based on two critical attributes, and applying the NBS and GNN-Explainer to identify significant connections.

73.37 ± 6.42 years) and gender (18 males and 41 females). The detailed data distribution can be found in Table 2. Below is a summary of the data acquisition process.

MRI data were obtained using a 3.0T MRI scanner (Signa, GE Healthcare, Milwaukee, Wisconsin) with a standard 8-channel head coil (HD 8Ch HiRes BRAIN ARRAY). Routine axial T1-weighted imaging (T1WI) was performed for structural imaging. Scanning was conducted from the top of the skull to the foramen magnum after alignment with the axial, coronal, and sagittal planes, using a spin echo (SE) sequence for T1WI. The specific scanning parameters were as follows: T1WI covered the entire brain, with a total of 20 slices; echo time (TE): 24 ms; repetition time (TR): 1900 ms; field of view (FOV): 24 × 24 cm; slice thickness/inter-slice gap: 5 mm/1.5 mm; number of excitations (NEX): 2; matrix: 320 × 224; and a scanning duration of 1 min and 37 s. Additionally, fMRI data were acquired using an echo planar imaging (EPI) sequence. The scanning parameters were as follows: 33 slices; TR: 2000 ms; TE: 30 ms; flip angle (FA): 90 degrees; slice thickness: 5 mm; inter-slice gap: 1 mm; scanning matrix: 64 × 64; and a total scanning time of 7 min.

ADNI (Alzheimer's Disease Neuroimaging Initiative) dataset

In addition to our In-house dataset, we incorporated data from the Alzheimer's Disease Neuroimaging Initiative (ADNI) dataset (adni.loni.usc.edu). The ADNI was launched in 2003 as a public–private partnership, led by Principal Investigator Michael W. Weiner, MD. The primary goal of ADNI has been to test whether serial magnetic resonance imaging (MRI), positron emission tomography (PET), other biological markers, and clinical and neuropsychological assessment can be combined to measure the progression of MCI and early AD. The ADNI phase protocols were approved by all the Institutional Review Boards of the participating institutions. Only data from volunteers who had provided written informed consent were used to complete these analyses. The ADNI4 protocols, received approval from the Advarra IRB (Protocol Pro00064250) on January 31, 2023. Specifically, we included all available paired T1WI MRI and fMRI data under AD conditions, along with corresponding APOE genotype information and MMSE scores. Additionally, demographic data were collected, including age (mean: 74.91 ± 7.91 years) and gender (59 males and 58 females). The detailed data distribution can be found in Table 2. Each collected MRI data was acquired from one of the following imaging sequences: MPRAGE SENSE2, MPRAGE S2 DIS3D, MPRAGE GRAPPA2, MPRAGE GRAPPA 2 ND, SAG MPRAGE NO ANGLE, Accelerated SAG IR-SPGR, or Sag IR-SPGR. Similarly, each collected fMRI data was obtained from one of the following modalities: Resting-State fMRI, Extended Resting-State fMRI, or Axial Resting-State fMRI (Eyes Open).

Table 2
Distribution of participants based on carriers status and cognitive impairment levels.

	Carriers				Non-Carriers			
	Total	Mild	Moderate	Severe	Total	Mild	Moderate	Severe
Overall	122	67	40	15	54	34	16	4
In-house	30	7	9	14	29	17	8	4
ADNI	92	60	31	1	25	17	8	0

The detailed comparison between the ADNI dataset and the in-house dataset is presented in Table 1.

Grouping Strategy

To examine the impact of APOE $\varepsilon 4$ on FC in AD across cognitive impairment levels, we categorized participants according to their APOE $\varepsilon 4$ carrier status and MMSE scores. APOE $\varepsilon 4$ carriers were defined as individuals with either the $\varepsilon 3/\varepsilon 4$ or $\varepsilon 4/\varepsilon 4$ genotypes, while non-carriers were those with other genotypes (Genin et al., 2011). Cognitive impairment levels were classified based on MMSE scores into three categories: severe (0–9), moderate (10–20), and mild (21–30) (Aye et al., 2024). Study comparison across different dimensions. First, differences between carriers and non-carriers were analyzed. Next, we compared three levels of cognitive impairment within the AD group and APOE $\varepsilon 4$ carrier group, respectively.

2.2. fMRI preprocessing

Noise, artifacts, and head motion during acquisition can easily affect fMRI data, making data preprocessing essential (Liu, 2016). To address these issues, this study employed the Gretna toolbox (Wang et al., 2015b), which integrates common preprocessing methods and facilitates batch processing and analysis. The specific preprocessing steps included removing unstable time points, slice timing correction, head motion correction, spatial normalization, detrending, regression of covariates, filtering, and removing time points with excessive head motion. Specifically, the first five time points of the fMRI data were removed, and the remaining data were band-pass filtered within the standard frequency range of 0.01–0.1 Hz (Wang et al., 2015b). Additionally, the Diffeomorphic Anatomical Registration Through Exponentiated Lie algebra (DARTEL) tool (Ashburner, 2007) was employed

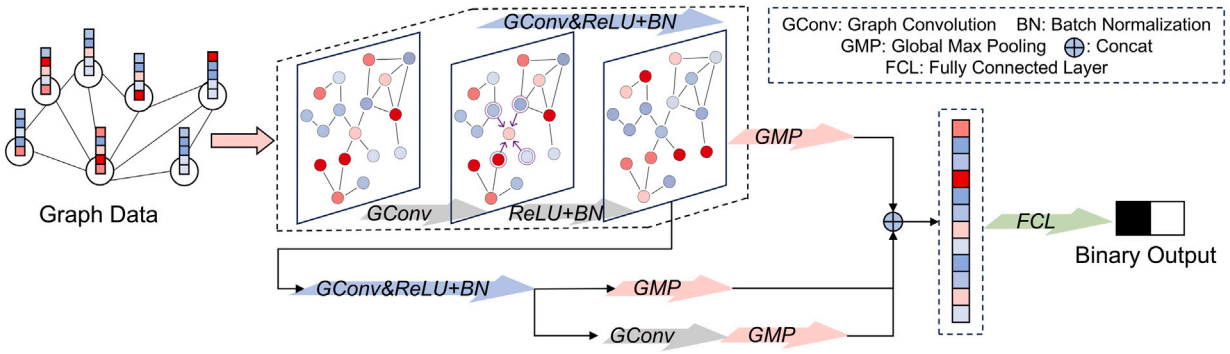

Fig. 2. The workflow of the GNN classification network begins with the input of graph data, consisting of FC matrices and node features, which is then processed by the network. The architecture includes three graph convolution layers, followed by global max pooling and fully connected layers, ultimately generating a binary output.

for normalization, utilizing the T1-weighted image for coregistration to enhance spatial accuracy. Other parameters followed the standard settings in Gretna.

The In-house dataset initially had dimensions of 64 × 64 × [25–36], with most scans having 210 time points. After preprocessing, including co-registration with T1 images and alignment to the MNI space, the spatial dimensions were standardized to 61 × 73 × 61, and the number of time points ranged from 75 to 205. Similarly, the ADNI dataset originally had dimensions of 64 × 64 × 48, with time points ranging from 140 to 200. After preprocessing and alignment to the same MNI space (61 × 73 × 61), the time points ranged from 82 to 200. This comprehensive preprocessing ensures that all fMRI images are standardized to a common scale and aligned with the MNI template.

2.3. FC construction and node feature extraction

After fMRI preprocessing, we parcel the voxels by defining regions of interest (ROIs). In this study, the Anatomical Automatic Labeling (AAL) parcellation template is used to divide the brain voxels into 90 ROIs, which are designated as brain network nodes. The averaged BOLD signal within each ROI is taken as the fMRI time series signal for each node. The FC between two brain network nodes is computed as the Pearson correlation coefficient between their fMRI time series. The functional brain network matrix is constructed by calculating the FC between all pairs of nodes. After FC construction, we applied a regression-out approach to remove any potential factors that might affect the statistical and classification results, such as sites, equipment, acquisition parameters, and the age and gender of participants (Gallo et al., 2023). Regression-out is a commonly used harmonization technique to address site effects and control for covariates across studies (Wang et al., 2023; Dansereau et al., 2017). This process resulted in harmonized FC matrices, which we subsequently used for further analysis.

Node features were extracted from the functional brain network matrix, providing a representation of the characteristics of each ROI. Key node feature metrics, including clustering coefficient, nodal efficiency, nodal local efficiency, degree centrality, and betweenness centrality, were selected for their relevance in exploring the interplay between brain structure and function in AD (Tijms et al., 2012; Lo et al., 2010; Wang et al., 2015a; Xue et al., 2014). The extraction of these features was performed using the Gretna Toolbox. A detailed explanation of each metric is provided below.

- Clustering Coefficient (Tijms et al., 2012)
  The clustering coefficient is a metric that is used to measure the degree of closeness between nodes in a network. The formula of the clustering coefficient is as follows:
  $$C_i = \frac{2 \cdot e_i}{k_i \cdot (k_i - 1)} \tag{1}$$
  where e_i is the number of edges that exist between neighbors of node i, and k_i is the degree of node i.
- Nodal Efficiency (Xue et al., 2014)
  The nodal efficiency quantifies the importance of the nodes for communication within the network. The nodes with high nodal efficiencies can be categorized as hubs in a network The formula is defined as:
  $$E_{\text{nodal}}(i) = \frac{1}{n-1} \sum_{j \neq i \in G} \frac{1}{L_{ij}} \tag{2}$$
  where G is a weighted graph (network), n is the total number of nodes in the network, L_{ij} is the shortest path length between nodes i and j.
- Nodal Local Efficiency (Xue et al., 2014)
  The local efficiency for a given node measures how efficient the communication is among the first neighbors of this node when it is removed. The formula is defined as:
  $$E_{local}(i) = \frac{1}{n} \sum_{i \in G} E_{global}(G_i) \tag{3}$$
  where G_i is the subgraph of neighbors of i, and the $E_{global}(G_i)$ is define as, representing the global efficiency:
  $$E_{\text{glob}}(G_i) = \frac{1}{n(n-1)} \sum_{j \neq i \in G} \frac{1}{L_{ij}} \tag{4}$$
- Degree Centrality (Tijms et al., 2012)
  Degree centrality D_i measures the importance of a node i by its number of connections:
  $$D_i = k_i \tag{5}$$
  where k_i is the degree of i.
- Betweenness Centrality (Tijms et al., 2012)
  Betweenness centrality B_i of node i quantifies its role as a bridge in the network:
  $$B_i = \sum_{a \neq b \in G} \frac{\sigma_{ab}(i)}{\sigma_{ij}} \tag{6}$$
  where σ_{ab} is the number of shortest paths between nodes a and b, and $\sigma_{ab}(i)$ is the number of those paths passing through i.

2.4. Statistical method

In the statistical test, we applied the NBS method (Zalesky et al., 2010), a statistical approach designed to identify significant differences in FC between comparison groups. We performed these comparisons by using the NBS toolbox (Zalesky et al., 2010). A two-sample t-test was employed to compare the FC matrices between the groups. To determine the significance of the observed differences, 5000 permutations were conducted. The significance threshold for identifying statistically significant subnetworks was $p < 0.05$.

2.5. GNN-explainer method

Although the NBS method has been widely applied, it remains insufficient for modeling complex high-order nonlinear characteristics, resulting in performance limitations (Yang et al., 2023, 2024). To better leverage these characteristics, the GNN-Explainer method was introduced in this study, comprising a Graph Neural Network (GNN) for classification and an Explainer module (Ying et al., 2019) for identifying FC features that contribute significantly to the classification task. Compared to other deep learning models, GNN is preferred for its capability to utilize the inherent graph structure of FC and incorporate graph theory metrics as node features. This combination facilitates the visualization of key features (Gallo et al., 2023). Specifically, the process began with training the GNN to perform binary classification on graph data, capturing high-order nonlinear connectivity relationships between brain regions (Yang et al., 2023). Subsequently, the Explainer module utilized the trained weights, graph data, and predictions to reveal the key brain connections driving the model's decisions, thereby identifying those critical for each comparison.

2.5.1. GNN classification network

The fundamental concept of graph convolution involves aggregating features from neighboring nodes and edges to produce new node representations. Building on this concept, a GNN-based classifier was developed, as illustrated in Fig. 2. The classifier takes graph data as input, consisting of an FC matrix and node features, and produces classification results as output. The FC matrix represents the relationships between all pairs of brain nodes, while the node features — such as clustering coefficient, nodal efficiency, nodal local efficiency, degree centrality, and betweenness centrality — capture the intrinsic properties of each node. The network then optimizes these feature representations, which are subsequently used for classification.

The network architecture comprises three graph convolutional layers, with the first two layers followed by ReLU activation and batch normalization. Each graph convolutional layer aggregates information from neighboring nodes and edges, effectively capturing local connectivity patterns. The layer dimensions are set to 128, 128, and 64, respectively, following parameter settings used in previous studies that employed interpretable GNN for brain network-based psychiatric diagnosis (Zheng et al., 2024). Global max pooling is applied at the end of each layer to extract the most salient features from all nodes, reducing dimensionality while preserving critical information. The pooled features from each graph convolutional layer are then concatenated, forming a feature vector that encapsulates multi-level representations of the graph. Subsequently, the concatenated features are fed into a fully connected layer for classification. Finally, the network is optimized using cross-entropy loss, a standard loss function for classification tasks.

2.5.2. Explainer module

The Explainer module is designed to elucidate the decisions made by the GNN classifier (Ying et al., 2019). It does so by generating explanations in the form of subgraphs that highlight the most crucial connections influencing the GNN's classifications. Specifically, these subgraphs are discovered through perturbations applied to the graph. The process involves randomly masking node features or edges in the graph and observing how these changes impact the model's predictions. A soft mask with continuous, learnable weights is employed to select the most relevant subgraph.

To generate robust and faithful explanations that align with the model's true behavior, the explainer module leverages multiple loss components to optimize the mask. These include prediction loss ($\mathcal{L}_{\text{pred}}$) to maintain the fidelity of the model's predictions, size loss ($\mathcal{L}_{\text{size}}$) to encourage sparsity in the mask, entropy loss ($\mathcal{L}_{\text{ent}}$) to promote diversity and avoid overfitting, and Laplacian loss ($\mathcal{L}_{\text{lap}}$) to preserve the smoothness of the graph structure. The final overall loss function is the sum of the following components:

$$\mathcal{L}_{\text{total}} = \mathcal{L}_{\text{pred}} + \mathcal{L}_{\text{size}} + \mathcal{L}_{\text{ent}} + \mathcal{L}_{\text{lap}} \tag{7}$$

Finally, the crucial connection subgraphs obtained from the two comparison groups were averaged to generate the final significant difference graph. This resulting averaged graph emphasizes the most consistent and important connections that distinguish the groups.

Table 3
Classification accuracy of GNN across different tasks. The results indicate consistently high performance of the GNN model in distinguishing between different comparison groups.

Comparison groups	Accuracy
Carriers vs Non-carriers	0.8507
All Mild vs All Moderate	0.6774[a]
All Mild vs All Severe	0.9565
All Moderate vs All Severe	0.9733
Carriers Mild vs Carriers Moderate	0.9156
Carriers Mild vs Carriers Severe	0.9500
Carriers Moderate vs Carriers Severe	0.9600

[a] Note: The All Mild vs All Moderate comparison was excluded from further analysis due to its relatively low accuracy.

2.6. Ablation study

To assess the significance of the functional connections identified by both the Explainer module and the NBS method, the ablation study was conducted. Specifically, we systematically masked each of the top 10 functional connections identified by both methods in every comparison. This masking process involved neutralizing the specific edges in the adjacency matrix corresponding to these connections, as well as the associated node features of the implicated brain regions. After each individual masking procedure, the GNN was rerun to evaluate how the removal of these masked connections affected the model's performance.

3. Experiments and results

This section presents the experimental results, including the classification performance achieved by GNN-Explainer and the identification of significant FCs using both the NBS and GNN-Explainer methods. To further evaluate the significance of the FCs identified by NBS and GNN-Explainer, the ablation study was conducted. Details of the experimental design and parameter settings can be found in the Supplementary Materials.

3.1. Classification performance

The classification performance of the GNN model was evaluated for multiple classification tasks, each designed to distinguish between different groups of AD patients based on APOE ε4 status and varying levels of cognitive impairment. The results are summarized in Table 3, showcasing the accuracy achieved in each classification scenario. The table demonstrates the effectiveness of the GNN model in classification, further supporting the utility of GNN-Explainer in capturing complex FC differences across groups.

3.2. Statistical and GNN-Explainer results comparing APOE ε4 carriers and non-carriers

The results of the NBS and GNN Explainer methods comparing APOE ε4 carriers and non-carriers are shown in Fig. 3. From Fig. 3, several influential network components for the classification of APOE ε4 carriers versus non-carriers can be identified, primarily composed of FCs between the parietal L and parietal R, prefrontal L and prefrontal R, as well as between occipital L and occipital R. The statistical results from NBS show significant changes in FCs between prefrontal R and temporal L, as well as between temporal L and temporal R for the carriers>non-carriers comparison.

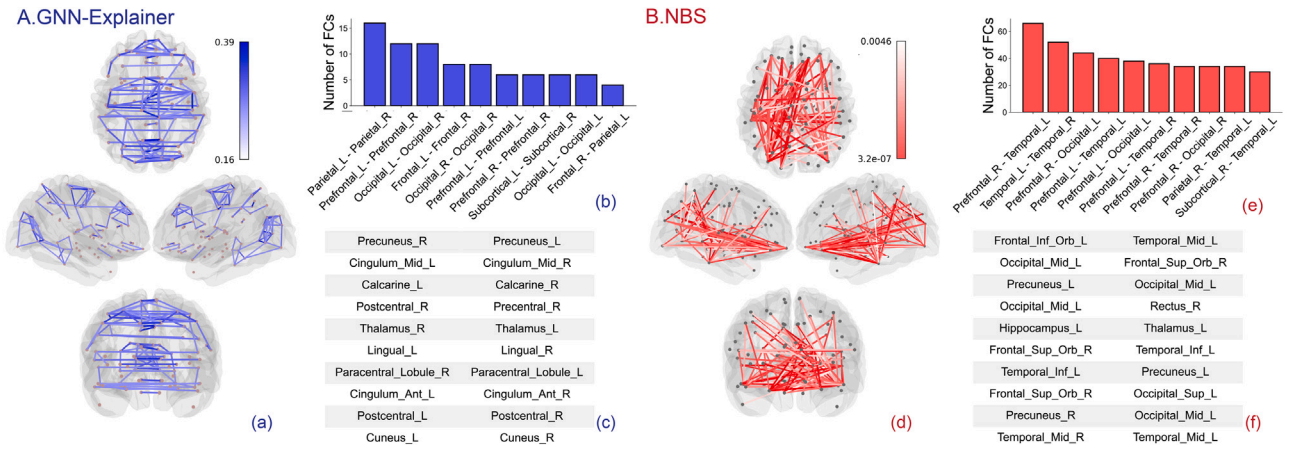

Fig. 3. Comparison of significant FCs between APOE $\varepsilon 4$ carriers and non-carriers using the GNN Explainer (A) and NBS (B) methods. Sub-figures (a, d) visualize the top 100 significant FCs from the left, right, front, and top perspectives, with an attached color bar. Sub-figures (b, e) display the distribution of significant FCs across anatomical pairs, ranked by the number of FCs in each pair. Sub-figure (b) includes the top 100 FCs identified by GNN-Explainer, while Sub-figure (e) includes the FCs with p-values < 0.05 identified by NBS. Sub-figures (c, f) list the top 10 most significant FCs for both methods.

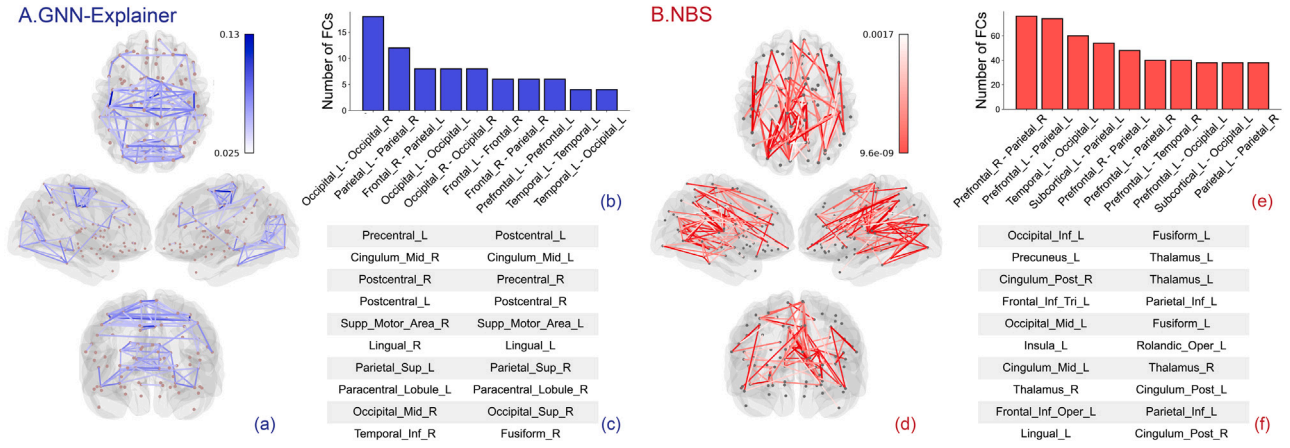

Fig. 4. Comparison of significant FCs between All Mild vs All Severe using the GNN Explainer (A) and NBS (B) methods. Sub-figures (a, d) visualize the top 100 significant FCs from the left, right, front, and top perspectives, with an attached color bar. Sub-figures (b, e) display the distribution of significant FCs across anatomical pairs, ranked by the number of FCs in each pair. Sub-figure (b) includes the top 100 FCs identified by GNN-Explainer, while Sub-figure (e) includes the FCs with p-values < 0.05 identified by NBS. Sub-figures (c, f) list the top 10 most significant FCs for both methods.

3.3. Statistical and GNN-Explainer results comparing different cognitive impairment levels of AD

Two comparisons were performed (All Mild vs All Severe and All Moderate vs All Severe) for different cognitive impairment levels of AD using both statistical and GNN-Explainer methods, with the results shown in Figs. 4 and 5, respectively.

For All Mild vs All Severe, the top 100 influential FCs were statistically compiled and visualized in Fig. 4. Several influential network components for the classification of Mild vs Severe AD can be identified, primarily consisting of FCs between the occipital L and occipital R, as well as between parietal L and parietal R. The statistical results from NBS show significant changes in network components composed of FCs between prefrontal R and parietal R, as well as between prefrontal L and parietal L, for the mild>severe comparison.

For All Moderate vs All Severe, the top 100 influential FCs were compiled statistics and visualized in Fig. 5. Influential network components were identified for the classification of Moderate vs Severe AD, which is primarily composed of FCs between the occipital L and occipital R. The statistical results using NBS show significant changes in network components composed of FCs between prefrontal R and parietal R as well as prefrontal L and parietal L for mild>severe comparison, which is consistent with those for mild vs severe.

3.4. Statistical and GNN-Explainer results comparing different cognitive impairment levels of AD in APOE $\varepsilon 4$ carriers

Three comparisons were performed (Carriers Mild vs Moderate, Carriers Mild vs Severe, and Carriers Moderate vs Severe) for different cognitive impairment levels of AD in APOE $\varepsilon 4$ carriers using both statistical and GNN-Explainer methods, with the results shown in Figs. 6, 7, and 8, respectively.

For Mild vs Severe in APOE $\varepsilon 4$ carriers (Fig. 6), influential network components for classification of Mild vs Severe AD in APOE $\varepsilon 4$ carriers were identified, which are primarily composed of FCs between the parietal L and parietal R, as well as FCs between occipital L and occipital R. The statistical results using NBS show significant changes in network components composed of FCs between prefrontal R and parietal R as well as prefrontal L and parietal L.

For Moderate vs Severe in APOE $\varepsilon 4$ carriers (Fig. 7), several influential network components for classification of Moderate vs Severe AD in APOE $\varepsilon 4$ carriers were identified, which are primarily composed of FCs between the occipital L and occipital R. The statistical results using NBS show significant changes in network components composed of FCs between prefrontal R and parietal R as well as prefrontal L and parietal L.

For Mild vs Moderate in APOE $\varepsilon 4$ carriers (Fig. 8), several influential network components for the classification of Mild vs Moderate AD in

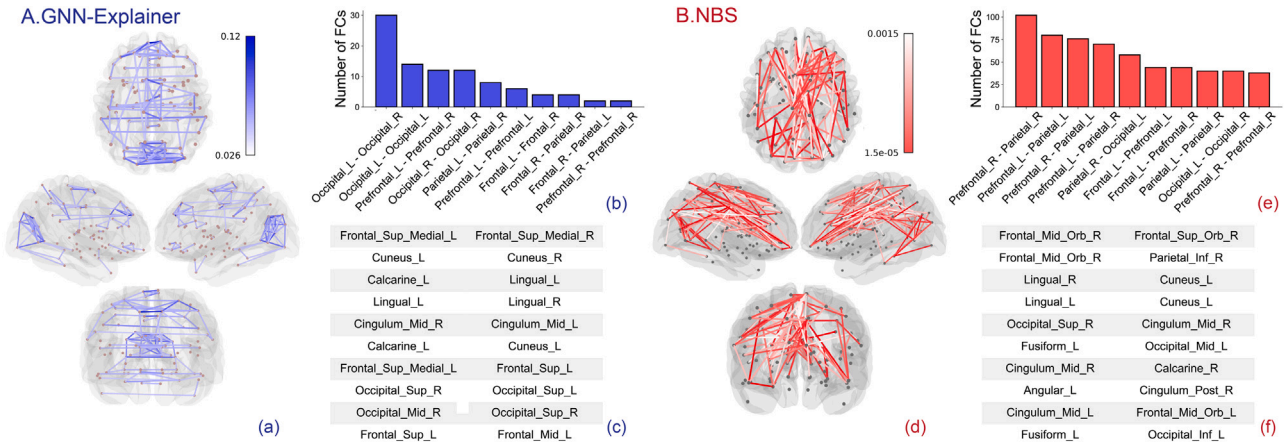

Fig. 5. Comparison of significant FCs between All Moderate vs All Severe using the GNN Explainer (A) and NBS (B) methods. Sub-figures (a, d) visualize the top 100 significant FCs from the left, right, front, and top perspectives, with an attached color bar. Sub-figures (b, e) display the distribution of significant FCs across anatomical pairs, ranked by the number of FCs in each pair. Sub-figure (b) includes the top 100 FCs identified by GNN-Explainer, while Sub-figure (e) includes the FCs with p-values < 0.05 identified by NBS. Sub-figures (c, f) list the top 10 most significant FCs for both methods.

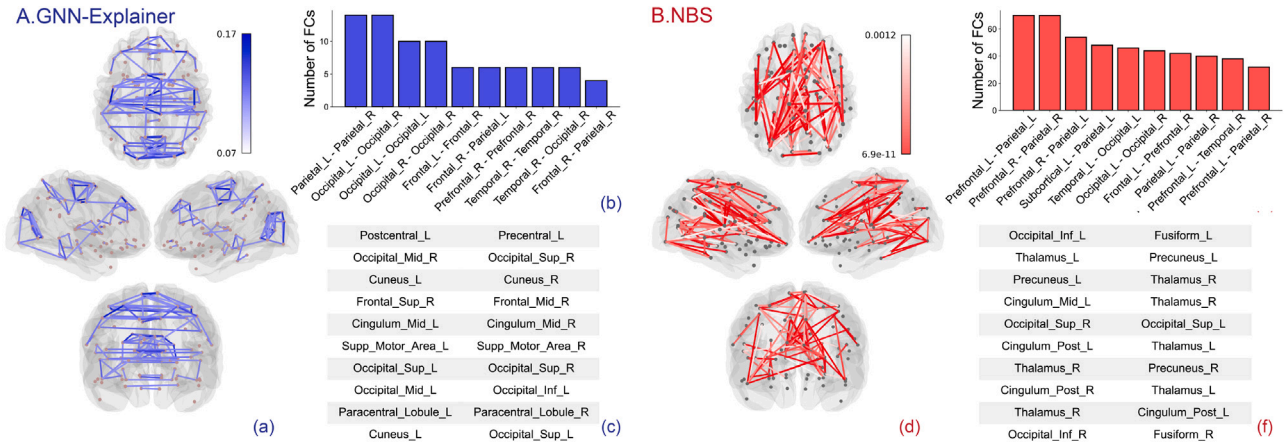

Fig. 6. Comparison of significant FCs between Mild vs Severe in APOE $\varepsilon 4$ carriers using the GNN Explainer (A) and NBS (B) methods. Sub-figures (a, d) visualize the top 100 significant FCs from the left, right, front, and top perspectives, with an attached color bar. Sub-figures (b, e) display the distribution of significant FCs across anatomical pairs, ranked by the number of FCs in each pair. Sub-figure (b) includes the top 100 FCs identified by GNN-Explainer, while Sub-figure (e) includes the FCs with p-values < 0.05 identified by NBS. Sub-figures (c, f) list the top 10 most significant FCs for both methods.

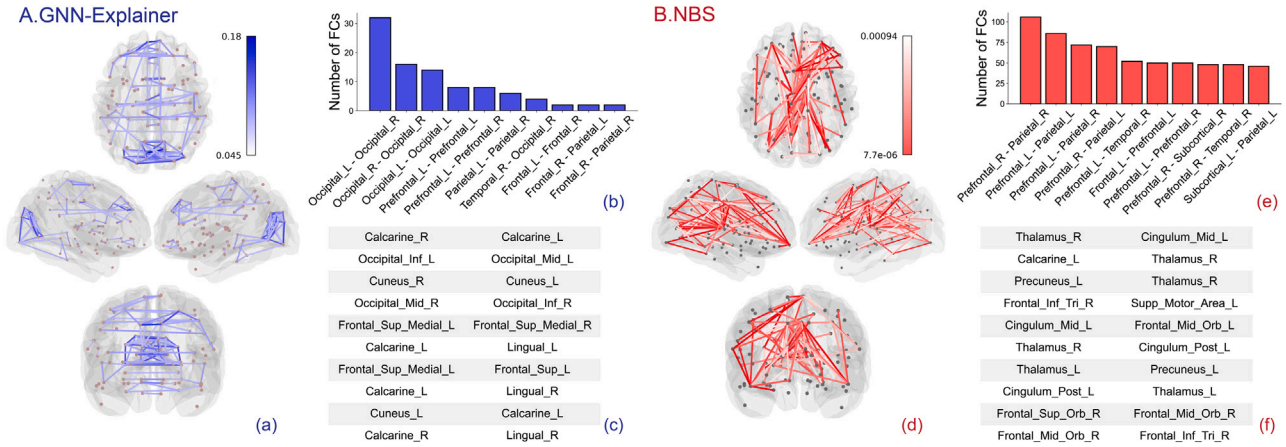

Fig. 7. Comparison of significant FCs between Moderate vs Severe in APOE $\varepsilon 4$ carriers using the GNN Explainer (A) and NBS (B) methods. Sub-figures (a, d) visualize the top 100 significant FCs from the left, right, front, and top perspectives, with an attached color bar. Sub-figures (b, e) display the distribution of significant FCs across anatomical pairs, ranked by the number of FCs in each pair. Sub-figure (b) includes the top 100 FCs identified by GNN-Explainer, while Sub-figure (e) includes the FCs with p-values < 0.05 identified by NBS. Sub-figures (c, f) list the top 10 most significant FCs for both methods.

Table 4
Summary of significant FCs identified by GNN Explainer and NBS methods in various comparison scenarios.

Comparison scenarios	Methods	Influential FCs in comparison
Carriers vs Non-carriers	GNNExplainer	parietal L-R; prefrontal L-R; occipital L-R
	NBS: Carriers>Non-carriers	prefrontal R-temporal L; temporal L-R
All Mild vs All Severe	GNNExplainer	occipital L-R; parietal L-R
	NBS: Mild>Severe	prefrontal R-parietal R; prefrontal L-parietal L
All Moderate vs All Severe	GNNExplainer	occipital L-R
	NBS: Moderate>Severe	prefrontal R-parietal R; prefrontal L-parietal L
Carriers Mild vs Carriers Severe	GNNExplainer	parietal L-R; occipital L-R
	NBS: Carriers Moderate>Carriers Severe	prefrontal R-parietal R; prefrontal L-parietal L
Carriers Moderate vs Carriers Severe	GNNExplainer	occipital L-R
	NBS: Carriers Moderate>Carriers Severe	prefrontal R-parietal R; prefrontal L-parietal L
Carriers Mild vs Carriers Moderate	GNNExplainer	occipital L-R; parietal L-R
	NBS: Carriers Mild>Carriers Moderate	/

APOE ε4 carriers can be identified, primarily consisting of FCs between the occipital L and occipital R, as well as between parietal L and parietal R. The statistical results from NBS show no significant changes.

3.5. Summary of the comparison results

The comparison results are summarized in Table 4.

For Carriers vs Non-carriers, classification is driven by stronger large-scale left–right brain FCs, including parietal L-R, prefrontal L-R, and occipital L-R. Statistical differences are also found primarily in left–right brain FCs, concentrated in prefrontal R-temporal L and temporal L-R.

Similarly, for the comparison of different cognitive impairment levels of AD, the classification is primarily driven by the occipital L-R and parietal L-R FCs, in which the importance of prefrontal L-R FCs becomes limited. From a statistical perspective, the prefrontal-parietal FCs (prefrontal R-parietal R, prefrontal L-parietal L) show main differences between milder levels of AD and severe AD.

3.6. Results of ablation study

As shown in Table 5, the accuracy metrics are presented after individually masking the pair of connections with the largest impact on performance, identified by both GNN-Explainer and NBS. The complete results for the top 10 connections can be found in the Supplementary Materials, Tables S2 and S3. From these results, the targeted removal of key connections led to a decrease in classification accuracy, highlighting their crucial role in maintaining model performance and differentiating between clinical groups. These findings emphasize the significance of these connections in functional connectivity analysis.

Furthermore, Table 5 corresponds closely with the findings presented in Table 4, as it lists the most influential connections that align with the anatomical pairs identified in each comparison. For example, in the comparison of Carriers vs Non-carriers, the most significant connections are found between Lingual R-Lingual L and Frontal Sup Orb R-Temporal Inf L, which are within the occipital L-R and parietal R-temporal L, respectively. In the analysis of All Mild vs All Severe, notable connections between Lingual R-Lingual L and Frontal Sup Orb R-Temporal Inf L belong to the occipital L-R and prefrontal L-parietal L, respectively.

4. Discussion

The complex effects of APOE ε4 and cognitive impairment levels of AD on brain networks of AD patients are not fully understood. Based on fMRI measurements, we explored key FC features influenced by these two factors using both statistical methods and an interpretable deep learning model, conducting multiple comparisons and classifications. We found that without considering cognitive levels, APOE ε4 primarily influenced FCs associated with the temporal lobe, but it influences different cognitive impairment levels of AD by adjusting prefrontal-parietal FCs. We will discuss the results as follows:

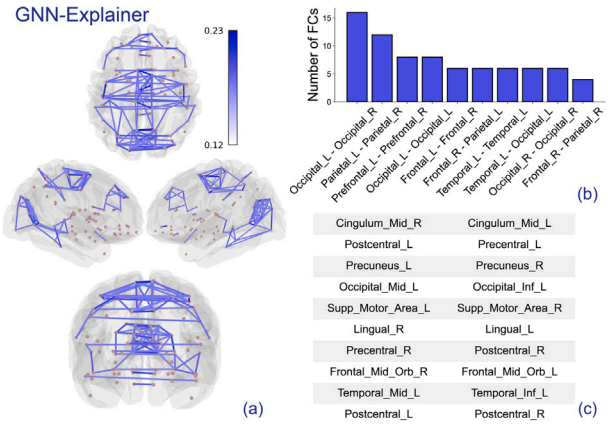

Fig. 8. Comparison of significant FCs between Mild vs Moderate in APOE ε4 carriers using the GNN Explainer (A) method. Sub-figures (a) visualize the top 100 significant FCs from the left, right, front, and top perspectives, with an attached color bar. Sub-figure (b) displays the distribution of significant FCs across anatomical pairs, ranked by the number of FCs in each pair, and includes the top 100 FCs identified by GNN-Explainer. Sub-figures (c) list the top 10 most significant FCs.

4.1. Classification performance and different results between statistical method and interpretable model

To the best of our knowledge, this is the first study to apply both the statistical method and the GNN-Explainer method in parallel, leveraging insights from two independent approaches. NBS processes adjacency matrices and performs two-sample one-tailed t-tests (e.g., Carriers < Non-Carriers and Carriers > Non-Carriers, separately) to primarily identify group differences. However, in our implementation, NBS consistently detects significant connections with $p < 0.05$ in a unidirectional manner, indicating that within each comparison, the overall FC strength either consistently increases or decreases across the group. On the other hand, the GNN-Explainer identifies FCs differences that represent the overall significant patterns. This process is driven by the high accuracy of GNN classification. Current GNN methods for AD prediction achieve an accuracy of 85% (Tekkesinoglu and Pudas, 2024). Consequently, results that surpass this accuracy threshold are considered appropriate for further in-depth analysis to uncover additional insights.

The overall classification performance highlights the model's robustness across various tasks, reinforcing the effectiveness of the Explainer module in identifying critical connections that significantly contribute to accuracy. The ablation study further supports these findings, revealing a notable drop in accuracy when the key connections identified by the GNN-Explainer are removed, thereby emphasizing their crucial role in the model's success.

Finally, we compared our findings with prior research on APOE ε4 and AD, which have identified key brain regions such as the insula,

Table 5
Accuracy metrics for the ablation study, showing the impact on model performance after masking the most influential connections identified by both GNN-Explainer and NBS. Each comparison displays the baseline accuracy alongside the accuracy after masking specific connections, highlighting a decrease in performance, which indicates the importance of these connections in the model's classification.

Method	Carriers vs None-carriers	Acc	All-Mild vs All-Severe	Acc
	Baseline	**0.8507**	Baseline	**0.9565**
GNN-Explainer	Lingual R-Lingual L	0.7208	Lingual R-Lingual L	0.8868
NBS	Frontal Sup Orb R-Temporal Inf L	0.7770	Frontal Inf Oper L-Parietal Inf L	0.8804
Method	All-Moderate vs All-Severe	Acc	Carriers Mild vs Carriers Severe	Acc
	Baseline	**0.9733**	Baseline	**0.9500**
GNN-Explainer	Calcarine L-Cuneus L	0.8886	Paracentral Lobule L-Paracentral Lobule R	0.8897
NBS	Angular L-Cingulum Post R	0.9314	Thalamus R-Precuneus R	0.8890
Method	Carriers Moderate vs Carriers Severe	Acc	Carriers Mild vs Carriers Moderate	Acc
	Baseline	**0.9600**	Baseline	**0.9156**
GNN-Explainer	Frontal Sup Medial L-Frontal Sup L	0.8291	Frontal Mid Orb R-Frontal Mid Orb L	0.8480
NBS	Frontal Mid Orb R-Frontal Inf Tri R	0.8455	/	/

cingulate cortex, and supplementary motor area (Wang et al., 2015a; Shi et al., 2020; Filippi et al., 2020). Consistent with these studies, our experimental comparisons revealed alterations in FC within these regions. For example, significant connections were observed in the cingulate cortex and insula in both the Mild vs Severe and Carriers vs Non-Carriers comparisons, while notable changes in the supplementary motor area were detected in the Moderate vs Severe comparison. We have provided only a few connections in this text; a comprehensive comparison of the regions we identified with those reported in previous studies can be found in Supplementary Table S4. Furthermore, when examining these regions at the anatomical level, previous studies have emphasized the involvement of the temporal, parietal, frontal, and occipital lobes (Filippi et al., 2020; Sethuraman et al., 2023). Our findings similarly revealed significant FC changes within these broader anatomical areas, such as the left–right parietal and left–right occipital regions, across different cognitive impairment levels of AD and between APOE $\varepsilon 4$ carriers and non-carriers. These results not only validate the identified brain regions but, more importantly, elucidate their crucial involvement in the progression of the disease.

4.2. APOE $\varepsilon 4$ primarily affects the FC of the temporal lobe

Our study disentangled the features associated with the cognitive impairment levels of AD and the APOE $\varepsilon 4$ factor in relation to FC. Our results indicate that the APOE $\varepsilon 4$ allele primarily selectively modulates the temporal cortex, consistent with previous research findings. The temporal cortex is a critical component of the posterior default mode network (DMN), and its function is typically associated with episodic memory (Greicius et al., 2003; Lou et al., 2004; Wagner et al., 2005). Machulda et al. (2011) found the reduced FC within the pDMN in APOE $\varepsilon 4$ carriers compared to non-carriers among older individuals. Demirtaş et al. (2017) found that significant FC differences in AD are primarily located in the left temporal lobe, likely influenced by the APOE $\varepsilon 4$ factor. Similarly, Wang et al. (2015a) found that the APOE $\varepsilon 4$ allele selectively modulates the pDMN and executive control network (ECN), and these changes largely account for the observed global differences in FC. It has been shown that the APOE $\varepsilon 4$ allele has a greater impact on memory retention for AD patients, while non-carriers exhibit greater impairment in tests of working memory, executive function, and language (Wolk et al., 2010). We hypothesize that the reduced FC, predominantly in the temporal lobe, may underlie the poorer memory performance observed in APOE $\varepsilon 4$ carriers.

4.3. The cognitive impairment levels of AD are primarily associated with the prefrontal-parietal FCs

The pathological features of AD are the accumulation of β-amyloid plaques and tau protein tangles, primarily located in the prefrontal and medial temporal lobes (Braak). Geschwind (Geschwind and Geschwind, 1974) originally introduced the concept of 'disconnection syndrome', referring to the disruption of connections between different brain regions caused by disease, resulting in cognitive dysfunction. Wang et al. (2007) found that, compared to healthy controls, AD patients exhibited decreased positive correlations between the prefrontal and parietal lobes, reporting a fronto-parietal disconnection phenomenon in AD patients. Using EEG, Hata et al. (2016) found that, compared to healthy controls, AD patients showed significantly reduced lagged phase synchrony in most cortical regions within the δ band. Additionally, lagged phase synchrony between the right dorsolateral prefrontal cortex (DLPFC) and the right posterior inferior parietal lobule (pIPL) was also reduced in the θ band. Consistent with previous studies, we found that FCs associated with the prefrontal cortex was the primary contributor to distinguishing between different severities of AD. Further, it is noteworthy that, from the internal classification results of carriers with varying cognitive impairment levels of AD, APOE $\varepsilon 4$ primarily affects prefrontal-parietal connectivity, thereby contributing to the development of AD. The unidirectional significant FCs identified in our statistical results also provided evidence in support of the disconnection hypothesis.

4.4. Interpreting brain connectivity with GNN-Explainer

The proposed GNN-Explainer comprises two key features: (1) graph convolutional layers in the GNN for population association studies, and (2) an explainer module for interpreting the model. These features offer advantages for the GNN-Explainer.

Firstly, graph convolutions act as low-pass filters (NT and Maehara, 2019). This process enables the model to uncover higher-order relationships present in population clusters that exhibit strong internal similarities. By representing population associations through graph structures, this method improves the distinction of brain network features in diverse populations, while also capturing inter-node dependencies (Yang et al., 2023). Second, the Explainer module provides the interpretation of the black-box GNN model, revealing significant differences between comparison groups. Although some applications of GNN have been used in tasks related to AD (Tekkesinoglu and Pudas, 2024; Song et al., 2019; Zhou et al., 2024), they rarely address the interpretability of the black-box GNN model, which further limits its potential for clinical applications. Building on these two features, GNN-Explainer uncovers clustering patterns and aggregates information from neighboring nodes, identifying significance subgraphs formed by FC clusters that highlight key structural divergences (Ying et al., 2019).

In this study, GNN-Explainer identifies large-scale left–right anatomical FC clusters, particularly within the occipital and parietal regions. This performs consistent with previous research. Gallo et al. (2023) employed GNN-Explainer to identify biomarkers and found intrinsic FCs within regions such as the thalamus and supramarginal gyrus in their study on depression. Similarly, Lei et al. (2022) used GNN to identify significant brain regions, which were predominantly located in subcortical and frontal regions, in patients with schizophrenia.

4.5. Defacts and future directions

Despite the valuable insights gained, this study has limitations. First, as a cross-sectional study, it provides only a single-time-point view of the brain's structural and functional state in AD patients. Longitudinal studies are necessary to capture the progression of these abnormalities over time and to examine their relationship to various stages of the disease (Filippi et al., 2020). Future research could greatly benefit from longitudinal data, enabling patient-specific analyses across different time points. Second, this analysis treated FC as a stationary feature; however, FC in the brain shows dynamic fluctuations that may offer additional insights into AD pathology. Future work should incorporate dynamic connectivity models to account for temporal variability in neural activity (Hutchison et al., 2013). Lastly, analyzing AD solely through an imaging modality limits the depth of understanding, given the complex nature of neurodegenerative disorders. Integrative, multi-modal approaches — incorporating molecular, genomic, physiological, and behavioral data — could more accurately represent the diverse facets of AD pathology, laying a more robust foundation for diagnostics and interventions (Gallo et al., 2023).

5. Conclusion

In this study, we combined statistical analysis methods and interpretable deep neural network methods to explore significant FC changes associated with APOE ε4 and cognitive impairment levels. The results showed that APOE ε4 primarily influenced temporal lobe FCs, but it influenced different cognitive impairment levels of AD by adjusting prefrontal-parietal FCs. The corresponding results not only supported the disconnection syndrome hypothesis of AD but also provided key data and evidence to address the question of how the APOE ε4 factor influences AD cognitive impairment levels through modulating brain FCs.

CRediT authorship contribution statement

Kangli Dong: Writing – original draft, Methodology, Formal analysis, Conceptualization. **Wei Liang:** Writing – original draft, Software, Investigation. **Ting Hou:** Validation, Formal analysis, Data curation. **Zhijie Lu:** Formal analysis, Data curation. **Yixuan Hao:** Formal analysis, Data curation. **Chenrui Li:** Formal analysis, Data curation. **Yue Qiu:** Formal analysis, Data curation. **Nan Kong:** Formal analysis, Data curation. **Yan Cheng:** Validation, Software. **Yaqi Wen:** Formal analysis, Data curation. **Wanyin Ma:** Formal analysis, Data curation. **Wenbin Zheng:** Formal analysis, Data curation. **Jitian Guan:** Formal analysis, Data curation. **Yan Lin:** Formal analysis, Data curation. **Kai Huang:** Formal analysis, Data curation. **Lu Zhang:** Validation, Software. **Siya Chen:** Visualization. **Xiangyuan Ma:** Writing – original draft, Formal analysis, Conceptualization. **Renhua Wu:** Writing – review & editing, Supervision, Resources, Funding acquisition, Data curation. **Naili Wei:** Writing – review & editing, Visualization, Resources, Funding acquisition, Data curation.

Funding

This work is supported by National Natural Science Foundation of China under grant 82001447, Guangdong Basic and Applied Basic Research Foundation, China under grant 2023A1515011488 and 2023B1515230008, Natural Science Foundation of Guangdong Provi nce, China under grant 2214050005144, Science and Technology of Guangdong Province, China under grant 210728166901906 and STKJ2021075. This work is also funded by Shantou University (STU Scientific Research Foundation for Talents, China: NTF24004T and NTF21004).

Declaration of competing interest

We declare that we have no financial and personal relationships with other people or organizations that can inappropriately influence our work, there is no professional or other personal interest of any nature or kind in any product, service and/or company that could be construed as influencing the position presented in, or the review of the manuscript.

Acknowledgments

A portion of the data collection and sharing for this project was funded by the Alzheimer's Disease Neuroimaging Initiative (ADNI) (National Institutes of Health Grant U01 AG024904) and DOD ADNI (Department of Defense award number W81XWH-12-2-0012). ADNI is funded by the National Institute on Aging, the National Institute of Biomedical Imaging and Bioengineering, and through generous contributions from the following: AbbVie, Alzheimer's Association; Alzheimer's Drug Discovery Foundation; Araclon Biotech; BioClinica, Inc.; Biogen; Bristol-Myers Squibb Company; CereSpir, Inc.; Cogstate; Eisai Inc.; Elan Pharmaceuticals, Inc.; Eli Lilly and Company; EuroImmun; F. Hoffmann-La Roche Ltd and its affiliated company Genentech, Inc.; Fujirebio; GE Healthcare; IXICO Ltd.; Janssen Alzheimer Immunotherapy Research & Development, LLC.; Johnson & Johnson Pharmaceutical Research & Development LLC.; Lumosity; Lundbeck; Merck & Co., Inc.; Meso Scale Diagnostics, LLC.; NeuroRx Research; Neurotrack Technologies; Novartis Pharmaceuticals Corporation; Pfizer Inc.; Piramal Imaging; Servier; Takeda Pharmaceutical Company; and Transition Therapeutics. The Canadian Institutes of Health Research is providing funds to support ADNI clinical sites in Canada. Private sector contributions are facilitated by the Foundation for the National Institutes of Health (www.fnih.org). The grantee organization is the Northern California Institute for Research and Education, and the study is coordinated by the Alzheimer's Therapeutic Research Institute at the University of Southern California. ADNI data are disseminated by the Laboratory for Neuro Imaging at the University of Southern California.

Appendix A. Supplementary data

Supplementary material related to this article can be found online at https://doi.org/10.1016/j.neuroimage.2024.120951.

Data and code availability statement

The in-house dataset supporting this study's findings is available from the corresponding author upon reasonable request. The public dataset supporting this study's findings is available from the Alzheimer's Disease Neuroimaging Initiative (ADNI) database (adni.loni.usc.edu).

References

Agosta, F., Vossel, K.A., Miller, B.L., Migliaccio, R., Bonasera, S.J., Filippi, M., Boxer, A.L., Karydas, A., Possin, K.L., Gorno-Tempini, M.L., 2009. Apolipoprotein E ε4 is associated with disease-specific effects on brain atrophy in Alzheimer's disease and frontotemporal dementia. Proc. Natl. Acad. Sci. 106 (6), 2018–2022.

Ashburner, J., 2007. A fast diffeomorphic image registration algorithm. Neuroimage 38 (1), 95–113.

Aye, S., Handels, R., Winblad, B., Jönsson, L., 2024. Optimising Alzheimer's disease diagnosis and treatment: assessing cost-utility of integrating blood biomarkers in clinical practice for disease-modifying treatment. J. Prev. Alzheimer's Dis. 1–15.

Bassett, D.S., Sporns, O., 2017. Network neuroscience. Nature Neurosci. 20 (3), 353–364.

Bertram, L., Lill, C.M., Tanzi, R.E., 2010. The genetics of Alzheimer disease: back to the future. Neuron 68 (2), 270–281.

Braak, H., Braak E (1995) Staging of Alzheimer's disease-related neurofibrillary changes. 271–278; discussion. Neurobiol. Aging 16, 278–284.
Brown, J.A., Terashima, K.H., Burggren, A.C., Ercoli, L.M., Miller, K.J., Small, G.W., Bookheimer, S.Y., 2011. Brain network local interconnectivity loss in aging APOE-4 allele carriers. Proc. Natl. Acad. Sci. 108 (51), 20760–20765.
Bullmore, E., Sporns, O., 2009. Complex brain networks: graph theoretical analysis of structural and functional systems. Nature Rev. Neurosci. 10 (3), 186–198.
Clarke, H., Messaritaki, E., Dimitriadis, S.I., Metzler-Baddeley, C., 2022. Dementia risk factors modify hubs but leave other connectivity measures unchanged in asymptomatic individuals: A graph theoretical analysis. Brain Connect. 12 (1), 26–40.
Corder, E.H., Saunders, A.M., Strittmatter, W.J., Schmechel, D.E., Gaskell, P.C., Small, G., Roses, A., Haines, J., Pericak-Vance, M.A., 1993. Gene dose of apolipoprotein E type 4 allele and the risk of Alzheimer's disease in late onset families. Science 261 (5123), 921–923.
Dai, Z., Lin, Q., Li, T., Wang, X., Yuan, H., Yu, X., He, Y., Wang, H., 2019. Disrupted structural and functional brain networks in Alzheimer's disease. Neurobiol. Aging 75, 71–82.
Dansereau, C., Benhajali, Y., Risterucci, C., Pich, E.M., Orban, P., Arnold, D., Bellec, P., 2017. Statistical power and prediction accuracy in multisite resting-state fMRI connectivity. Neuroimage 149, 220–232.
Delbeuck, X., Van der Linden, M., Collette, F., 2003. Alzheimer'disease as a disconnection syndrome? Neuropsychol. Rev. 13, 79–92.
Demirtaş, M., Falcon, C., Tucholka, A., Gispert, J.D., Molinuevo, J.L., Deco, G., 2017. A whole-brain computational modeling approach to explain the alterations in resting-state functional connectivity during progression of Alzheimer's disease. NeuroImage: Clin. 16, 343–354.
Filippi, M., Basaia, S., Canu, E., Imperiale, F., Magnani, G., Falautano, M., Comi, G., Falini, A., Agosta, F., 2020. Changes in functional and structural brain connectome along the Alzheimer's disease continuum. Mol. Psychiatry 25 (1), 230–239.
Filippini, N., MacIntosh, B.J., Hough, M.G., Goodwin, G.M., Frisoni, G.B., Smith, S.M., Matthews, P.M., Beckmann, C.F., Mackay, C.E., 2009. Distinct patterns of brain activity in young carriers of the APOE-ε4 allele. Proc. Natl. Acad. Sci. 106 (17), 7209–7214.
Fleisher, A.S., Sherzai, A., Taylor, C., Langbaum, J.B., Chen, K., Buxton, R.B., 2009. Resting-state BOLD networks versus task-associated functional MRI for distinguishing Alzheimer's disease risk groups. Neuroimage 47 (4), 1678–1690.
Gallo, S., El-Gazzar, A., Zhutovsky, P., Thomas, R.M., Javaheripour, N., Li, M., Bartova, L., Bathula, D., Dannlowski, U., Davey, C., et al., 2023. Functional connectivity signatures of major depressive disorder: machine learning analysis of two multicenter neuroimaging studies. Mol. Psychiatry 28 (7), 3013–3022.
Genin, E., Hannequin, D., Wallon, D., Sleegers, K., Hiltunen, M., Combarros, O., Bullido, M.J., Engelborghs, S., De Deyn, P., Berr, C., et al., 2011. APOE and Alzheimer disease: a major gene with semi-dominant inheritance. Mol. Psychiatry 16 (9), 903–907. http://dx.doi.org/10.1038/mp.2011.52.
Geschwind, N., Geschwind, N., 1974. Disconnexion Syndromes in Animals and Man. Springer.
Goryawala, M., Duara, R., Loewenstein, D.A., Zhou, Q., Barker, W., Adjouadi, M., Alzheimer's Disease Neuroimaging Initiative, et al., 2015. Apolipoprotein-E4 (ApoE4) carriers show altered small-world properties in the default mode network of the brain. Biomed. Phys. Eng. Express 1 (1), 015001.
Goveas, J.S., Xie, C., Chen, G., Li, W., Ward, B.D., Franczak, M.B., Jones, J.L., Antuono, P.G., Li, S.J., 2013. Functional network endophenotypes unravel the effects of apolipoprotein E epsilon 4 in middle-aged adults. PLoS One 8 (2), e55902.
Greicius, M.D., Krasnow, B., Reiss, A.L., Menon, V., 2003. Functional connectivity in the resting brain: a network analysis of the default mode hypothesis. Proc. Natl. Acad. Sci. 100 (1), 253–258.
Hata, M., Kazui, H., Tanaka, T., Ishii, R., Canuet, L., Pascual-Marqui, R.D., Aoki, Y., Ikeda, S., Kanemoto, H., Yoshiyama, K., et al., 2016. Functional connectivity assessed by resting state EEG correlates with cognitive decline of Alzheimer's disease–An eLORETA study. Clin. Neurophysiol. 127 (2), 1269–1278.
Hutchison, R.M., Womelsdorf, T., Allen, E.A., Bandettini, P.A., Calhoun, V.D., Corbetta, M., Della Penna, S., Duyn, J.H., Glover, G.H., Gonzalez-Castillo, J., et al., 2013. Dynamic functional connectivity: promise, issues, and interpretations. Neuroimage 80, 360–378.
John, M., Ikuta, T., Ferbinteanu, J., 2017. Graph analysis of structural brain networks in Alzheimer's disease: beyond small world properties. Brain Struct. Funct. 222, 923–942.
Koelewijn, L., Lancaster, T.M., Linden, D., Dima, D.C., Routley, B.C., Magazzini, L., Barawi, K., Brindley, L., Adams, R., Tansey, K.E., et al., 2019. Oscillatory hyperactivity and hyperconnectivity in young APOE-ε4 carriers and hypoconnectivity in Alzheimer's disease. Elife 8, e36011.
Lei, D., Qin, K., Pinaya, W.H.L., Young, J., Van Amelsvoort, T., Marcelis, M., Donohoe, G., Mothersill, D.O., Corvin, A., Vieira, S., Lui, S., Scarpazza, C., Arango, C., Bullmore, E., Gong, Q., McGuire, P., Mechelli, A., 2022. Graph convolutional networks reveal network-level functional dysconnectivity in Schizophrenia. Schizophr. Bull. 48 (4), 881–892. http://dx.doi.org/10.1093/schbul/sbac047, URL: https://academic.oup.com/schizophreniabulletin/article/48/4/881/6586020.
Liu, T.T., 2016. Noise contributions to the fMRI signal: An overview. Neuroimage 143, 141–151. http://dx.doi.org/10.1016/j.neuroimage.2016.09.008, URL: https://www.sciencedirect.com/science/article/pii/S1053811916304694.
Liu, C.C., Kanekiyo, T., Xu, H., Bu, G., 2013. Apolipoprotein E and Alzheimer disease: risk, mechanisms and therapy. Nat. Rev. Neurol. 9 (2), 106–118.
Lo, C.Y., Wang, P.N., Chou, K.H., Wang, J., He, Y., Lin, C.P., 2010. Diffusion tensor tractography reveals abnormal topological organization in structural cortical networks in Alzheimer's disease. J. Neurosci. 30 (50), 16876–16885.
Lou, H.C., Luber, B., Crupain, M., Keenan, J.P., Nowak, M., Kjaer, T.W., Sackeim, H.A., Lisanby, S.H., 2004. Parietal cortex and representation of the mental self. Proc. Natl. Acad. Sci. 101 (17), 6827–6832.
Ma, C., Wang, J., Zhang, J., Chen, K., Li, X., Shu, N., Chen, Y., Liu, Z., Zhang, Z., 2017. Disrupted brain structural connectivity: pathological interactions between genetic APOE ε4 status and developed MCI condition. Mol. Neurobiol. 54, 6999–7007.
Machulda, M.M., Jones, D.T., Vemuri, P., McDade, E., Avula, R., Przybelski, S., Boeve, B.F., Knopman, D.S., Petersen, R.C., Jack, C.R., 2011. Effect of APOE ε4 status on intrinsic network connectivity in cognitively normal elderly subjects. Arch. Neurol. 68 (9), 1131–1136.
Mirza-Davies, A., Foley, S., Caseras, X., Baker, E., Holmans, P., Escott-Price, V., Jones, D.K., Harrison, J.R., Messaritaki, E., 2022. The impact of genetic risk for Alzheimer's disease on the structural brain networks of young adults. Front. Neurosci. 16, 987677.
NT, H., Maehara, T., 2019. Revisiting graph neural networks: All we have is low-pass filters. arXiv:1905.09550, URL: https://arxiv.org/abs/1905.09550.
Sanabria-Diaz, G., Martinez-Montes, E., Melie-Garcia, L., Alzheimer's Disease Neuroimaging Initiative, 2013. Glucose metabolism during resting state reveals abnormal brain networks organization in the Alzheimer's disease and mild cognitive impairment. PLoS One 8 (7), e68860.
Sethuraman, S.K., Malaiyappan, N., Ramalingam, R., Basheer, S., Rashid, M., Ahmad, N., 2023. Predicting Alzheimer's disease using deep neuro-functional networks with resting-state fMRI. Electronics 12 (4), 1031.
Shi, J.Y., Wang, P., Wang, B.H., Xu, Y., Chen, X., Li, H.J., 2020. Brain homotopic connectivity in mild cognitive impairment APOE-ε4 carriers. Neuroscience 436, 74–81.
Song, T.A., Chowdhury, S.R., Yang, F., Jacobs, H., Fakhri, G.E., Li, Q., Johnson, K., Dutta, J., 2019. Graph convolutional neural networks for Alzheimer's disease classification. In: 2019 IEEE 16th International Symposium on Biomedical Imaging. ISBI 2019, pp. 414–417. http://dx.doi.org/10.1109/ISBI.2019.8759531.
Stam, C.J., Jones, B., Nolte, G., Breakspear, M., Scheltens, P., 2007. Small-world networks and functional connectivity in Alzheimer's disease. Cerebral Cortex 17 (1), 92–99.
Tekkesinoglu, S., Pudas, S., 2024. Explaining graph convolutional network predictions for clinicians—An explainable AI approach to Alzheimer's disease classification. Frontiers Artificial Intelligence 6, 1334613.
Therriault, J., Schindler, S.E., Salvadó, G., Pascoal, T.A., Benedet, A.L., Ashton, N.J., Karikari, T.K., Apostolova, L., Murray, M.E., Verberk, I., et al., 2024. Biomarker-based staging of Alzheimer disease: rationale and clinical applications. Nat. Rev. Neurol. 20 (4), 232–244.
Tijms, B.M., Seriès, P., Willshaw, D.J., Lawrie, S.M., 2012. Similarity-based extraction of individual networks from gray matter MRI scans. Cerebral Cortex 22 (7), 1530–1541.
Van der Flier, W., Schoonenboom, S., Pijnenburg, Y., Fox, N., Scheltens, P., 2006. The effect of APOE genotype on clinical phenotype in Alzheimer disease. Neurology 67 (3), 526–527.
Wagner, A.D., Shannon, B.J., Kahn, I., Buckner, R.L., 2005. Parietal lobe contributions to episodic memory retrieval. Trends Cogn. Sci. 9 (9), 445–453.
Wang, Y.W., Chen, X., Yan, C.G., 2023. Comprehensive evaluation of harmonization on functional brain imaging for multisite data-fusion. Neuroimage 274, 120089.
Wang, K., Liang, M., Wang, L., Tian, L., Zhang, X., Li, K., Jiang, T., 2007. Altered functional connectivity in early Alzheimer's disease: A resting-state fMRI study. Hum. Brain Mapp. 28 (10), 967–978.
Wang, J., Wang, X., He, Y., Yu, X., Wang, H., He, Y., 2015a. Apolipoprotein E ε4 modulates functional brain connectome in Alzheimer's disease. Hum. Brain Mapp. 36 (5), 1828–1846.
Wang, J., Wang, X., Xia, M., Liao, X., Evans, A., He, Y., 2015b. GRETNA: a graph theoretical network analysis toolbox for imaging connectomics. Front. Hum. Neurosci. 9, http://dx.doi.org/10.3389/fnhum.2015.00386, URL: https://www.frontiersin.org/journals/human-neuroscience/articles/10.3389/fnhum.2015.00386.
Wang, J., Zuo, X., Dai, Z., Xia, M., Zhao, Z., Zhao, X., Jia, J., Han, Y., He, Y., 2013. Disrupted functional brain connectome in individuals at risk for Alzheimer's disease. Biol. Psychiatry 73 (5), 472–481.
Wolk, D.A., Dickerson, B.C., Alzheimer's Disease Neuroimaging Initiative, Weiner, M., Aiello, M., Aisen, P., Albert, M.S., Alexander, G., Anderson, H.S., Anderson, K., et al., 2010. Apolipoprotein E (APOE) genotype has dissociable effects on memory and attentional–executive network function in Alzheimer's disease. Proc. Natl. Acad. Sci. 107 (22), 10256–10261.
Xue, K., Luo, C., Zhang, D., Yang, T., Li, J., Gong, D., Chen, L., Medina, Y.I., Gotman, J., Zhou, D., et al., 2014. Diffusion tensor tractography reveals disrupted structural connectivity in childhood absence epilepsy. Epilepsy Res. 108 (1), 125–138.
Yang, Y., Ye, C., Guo, X., Wu, T., Xiang, Y., Ma, T., 2024. Mapping multi-modal brain connectome for brain disorder diagnosis via cross-modal mutual learning. IEEE Trans. Med. Imaging 43 (1), 108–121. http://dx.doi.org/10.1109/TMI.2023.3294967.

Yang, Y., Ye, C., Ma, T., 2023. A deep connectome learning network using graph convolution for connectome-disease association study. Neural Netw. 164, 91–104. http://dx.doi.org/10.1016/j.neunet.2023.04.025, URL: https://www.sciencedirect.com/science/article/pii/S0893608023002113.

Ying, Z., Bourgeois, D., You, J., Zitnik, M., Leskovec, J., 2019. Gnnexplainer: Generating explanations for graph neural networks. Adv. Neural Inf. Process. Syst. 32.

Zalesky, A., Fornito, A., Bullmore, E.T., 2010. Network-based statistic: Identifying differences in brain networks. Neuroimage 53 (4), 1197–1207. http://dx.doi.org/10.1016/j.neuroimage.2010.06.041, URL: https://www.sciencedirect.com/science/article/pii/S1053811910008852.

Zheng, K., Yu, S., Chen, B., 2024. CI-GNN: A Granger causality-inspired graph neural network for interpretable brain network-based psychiatric diagnosis. Neural Netw. 172, 106147. http://dx.doi.org/10.1016/j.neunet.2024.106147, URL: https://linkinghub.elsevier.com/retrieve/pii/S0893608024000716.

Zhou, Z., Wang, Q., An, X., Chen, S., Sun, Y., Wang, G., Yan, G., 2024. A novel graph neural network method for Alzheimer's disease classification. Comput. Biol. Med. 180, 108869. http://dx.doi.org/10.1016/j.compbiomed.2024.108869, URL: https://www.sciencedirect.com/science/article/pii/S0010482524009545.